

Nanoscale

Accepted Manuscript



This is an *Accepted Manuscript*, which has been through the Royal Society of Chemistry peer review process and has been accepted for publication.

Accepted Manuscripts are published online shortly after acceptance, before technical editing, formatting and proof reading. Using this free service, authors can make their results available to the community, in citable form, before we publish the edited article. We will replace this *Accepted Manuscript* with the edited and formatted *Advance Article* as soon as it is available.

You can find more information about *Accepted Manuscripts* in the [Information for Authors](#).

Please note that technical editing may introduce minor changes to the text and/or graphics, which may alter content. The journal's standard [Terms & Conditions](#) and the [Ethical guidelines](#) still apply. In no event shall the Royal Society of Chemistry be held responsible for any errors or omissions in this *Accepted Manuscript* or any consequences arising from the use of any information it contains.

Novel design of ultra-fast Si anodes for Li-ion batteries: crystalline Si@amorphous Si encapsulating hard carbon

Cite this: DOI: 10.1039/x0xx00000x

Received 00th January 2012,
Accepted 00th January 2012

DOI: 10.1039/x0xx00000x

www.rsc.org/

Chanhoon Kim,^a Minseong Ko,^a Seungmin Yoo,^a Sujong Chae,^a Sinho Choi,^a Eun-Ho Lee,^b Seunghee Ko,^a Sang-Young Lee,^a Jaephil Cho*^a and Soojin Park*^a

Nanocrystalline Si (c-Si) dispersed in amorphous Si (a-Si) encapsulating hard carbon (HC) has been synthesized as an anode material for fast chargeable lithium-ion batteries. The HC derived from natural polysaccharide was coated by thin a-Si layer through chemical vapour deposition (CVD) using silane (SiH₄) as a precursor gas. The HC@c-Si@a-Si anodes showed excellent cycle retention of 97.8 % even after 200 cycles at a 1 C discharge/charge rate. Furthermore, high capacity retention of ~54 % of its initial reversible capacity at 0.2 C rate was obtained at a high discharge/charge rate of 5 C. Moreover, LiCoO₂/HC@c-Si@a-Si full-cell showed excellent rate capability and very stable long-term cycle. Even at a rate of 10 C discharge/charge, the capacity retention of the LiCoO₂/HC@c-Si@a-Si full-cell was 50.8% of its capacity at a rate of 1 C discharge/charge and showed superior cycle retention of 80 % after 160 cycles at a rate of 1 C discharge/charge.

1. Introduction

Recently, growing interest in electric vehicles (EVs) due to rapidly rising price of petroleum and growing concern of global warming has brought attention to the lithium-ion batteries (LIBs) more and more.¹ However, conventional graphite anodes, which are the most widely used anode material in LIBs, cannot deliver sufficient theoretical capacity (< 372 mAh g⁻¹) and meet the requirements for increasing mobility and high energy demands.^{2,3} Therefore, alternative anode materials with high energy and high power density are urgently needed for the next generation LIBs.

Among the promising anode materials which have been studied in recent years, silicon (Si) has attracted considerable interest as an anode material for the next generation LIBs owing to its several advantages including: a) the highest theoretical gravimetric capacity (3580 mAh g⁻¹ for Li₁₅Si₄ at room temperature), b) a relatively low lithium reaction potential (< 0.4 vs. Li/Li⁺), c) a low cost, and d) environmentally friendliness.⁴⁻⁶ However, the insertion of Li⁺ into Si leads to large volume expansion of >300% at fully lithiated state (Li_{3.75}Si at room temperature).^{1,7,8} This huge volume expansion causes destruction of its structure and generates secondary particles which are delamination from the current collector or from other conductive phases (conductive agent or binder).⁹ Moreover, continuous destruction of Si during cycling impedes formation of stable solid electrolyte interphase (SEI) layer which inhibits further electrolyte decomposition.⁶ Consequently, serious capacity degradation of Si appears at the early cycles.

To solve above problems, tremendous efforts have been proposed such as designing Si nanostructures (*e.g.*, nanoparticles, nanowires, nanotubes, *etc.*) and their composites with others (*e.g.*, metal oxide, carbonaceous materials, inactive metals, *etc.*).^{8,11-18} In

particular, nanostructured Si/C composites and core-shell structures combine high capacity provided by Si with the high electrical conductivity, long cycle life, and good rate performance by carbon.¹⁹⁻²⁵

Meanwhile, amorphous Si (a-Si) has also intensively studied as an anode material for the next generation LIBs because of its large critical size for fracture and lithiation reaction velocity comparable to the crystalline Si (c-Si).²⁶⁻³⁰ Cui's group recently demonstrated that the lithiation/delithiation kinetics of a-Si nanospheres were observed by in-situ transmission electron microscopy (TEM).³¹ According to their results, the critical size for destruction of a-Si is much larger than c-Si and the lithiation reaction velocity is not slow as c-Si. These results suggest that a-Si undergoes smaller physical transformations than c-Si during the first cycle. Tritsarlis et al. calculated energy barriers for the lithium diffusion in a-Si and confirmed that a-Si have several pathways of relatively lower energy barriers (<0.5 eV) for the lithium diffusion than c-Si.²⁹ Therefore, use of a-Si can be more reasonable choice for the next LIBs.

Herein, we demonstrate a novel design of Si/C composite material consisting of the c-Si nanodomains dispersed in a-Si encapsulating hard carbon (HC). We successfully synthesized hard carbon by a simple carbonization process of natural polysaccharide, agarose, and demonstrate the superior electrochemical performance of HC, compared to natural graphite anodes. Subsequently, we adopt thin a-Si layer on the HC surface using silane gas via CVD process and followed by carbon coating on the surface of HC/a-Si composite. During the carbon coating, a-Si was partially converted nano-sized c-Si domains which were uniformly dispersed in a-Si. This HC@c-Si@a-Si core-shell structure delivers a specific capacity of ~54% even at high rate of 5 C discharge/charge compared to reversible capacity at 0.2 C and maintains long term cycle stability

with 97.8% (compared to the first cycle) of capacity retention after 200 cycles at a rate of 1 C discharge/charge. Furthermore, capacity of the LiCoO₂/HC@c-Si@a-Si full-cell at a high rate of 10 C discharge/charge is approximately half (50.8%) of its capacity at a rate of 1 C discharge/charge and shows more stable cycle retention of 80 % after 160 cycles at a rate of 1 C discharge/charge.

2. Result and Discussion

2.1. Synthesis of hard carbon from natural polysaccharide

Hard carbon (HC) was synthesized via a simple carbonization process (900 °C for 2 h in argon environment) of agarose hydrogel (Fig. 1a). Agarose is one type of the natural polysaccharides that are easily extracted from seaweeds and also environmental friendly material. The molecular structure of agarose is quite similar to that of cellulose which delivers microporous structure during carbonization process.³²

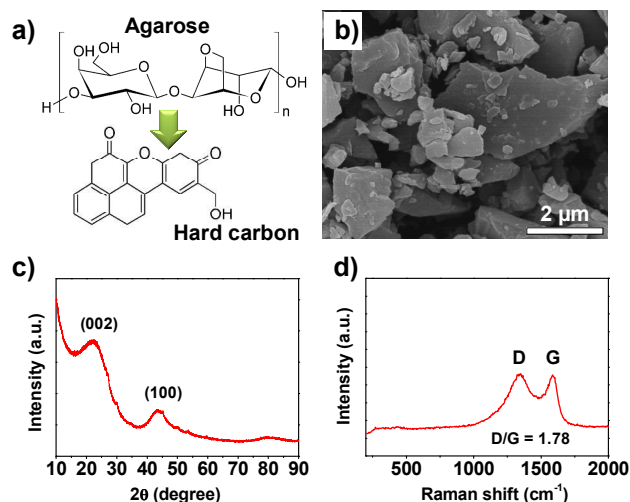


Fig. 1 Characterization of HC. a) Carbonization of agarose polymer; b) SEM image of as-synthesized HC; c) XRD pattern and d) Raman spectrum of as-synthesized HC.

Scanning electron microscopy (SEM) image of as-synthesized HC is shown in Fig. 1b. The micrometre-sized HC particles show flake-type structure. The X-ray Diffraction (XRD) pattern of the HC shows the diffraction peaks at 22.5° and 43.5° which correspond to the lattice planes (002) and (100) of the amorphous nature of obtained materials, respectively (Fig. 1c).³³ The inter-layer spacing of the HC is about 0.390 nm (corresponded to (002)) which is the larger interlayer spacing compared to pure graphite carbon (about 0.33 nm), which is considered to be favourable for lithium insertion and extraction, maintaining the structural durability of an electrode during cycles.^{32,34}

To investigate the carbon quality of the HC particles, we obtained Raman spectrum (Fig. 1d). The HC exhibits two peaks at around 1350 and 1585 cm⁻¹, which are attributed to the D and G bands of carbon, respectively.^{20,35} The D band corresponds to the structural defects and disorder of carbon, while the G band corresponds to the stretching vibration mode of graphite crystals.³³ The D band is not observed in perfect graphite crystals and only appears in the presence of disorder.³⁶ The peak integrated intensity ratio of the D band to the G band (D/G) for HC is estimated to be 1.78, indicating that most of carbon species in the HC are amorphous.^{7,37}

2.2. Electrochemical performances of HC anode

A series of electrochemical characterizations were carried out to investigate the electrochemical properties of the HC electrodes in a coin-type half-cell (2016 R-type). The first discharge and charge of HC electrode were carried out in the voltage range of 0.005–2.0 V at a rate of 0.05 C (corresponding to 17 mA/g), as shown in Fig. 2a. The discharge and charge capacities reach 667.6 and 501.2 mAh g⁻¹ with the initial coulombic efficiency (ICE) of 75.1%. Reactions between lithium ion and hard carbon are observed from 1.25 V to 0.15 V in the first cycle of the HC and the low voltage plateau appeared under 0.1 V.

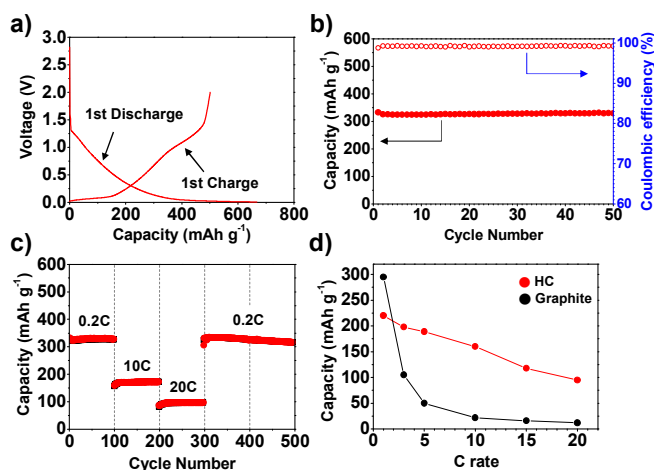


Fig. 2 Electrochemical performances of the HC anode. (a) First discharge/charge curves of the HC at a rate of 0.05 C between 0.005 V and 2.0 V; the cycle performances of the HC (b) at a rate of 0.2 C discharge/charge, and (c) at various discharge/charge rates (0.2 C, 10 C, and 20 C) between 0.01 V and 2.0 V; (d) Rate capabilities between HC and natural graphite (the same discharge/charge rate from 1 to 20 C).

This characteristic behaviour of the HC during the first cycle is correlated to their disordered and microporous structure.^{38,39} Dahn et al. suggested that the inserted lithium in hard carbon could transfer part of its 2s electron (in a covalent bond) to a neighbouring hydrogen. This would cause changes in the relative atomic positions of the C and H, resulting in the hysteresis.⁴⁰ The low voltage plateau, occurring under 0.1 V, has been explained by the formation of lithium metal clusters inside the nanopores.⁴¹ The HC shows stable cycle retention at 0.2 C (corresponding to 66 mA g⁻¹) as well as excellent rate capability even at a very high rate of 20 C (corresponding to 6600 mA g⁻¹) (Fig. 2b and c). Notably, even after 500 cycles at various discharge/charge rate (0.2/0.2 C, 10/10 C, 20/20 C), specific capacity of 316 mAh g⁻¹ is obtained with retention of 95.2 % with high CE (approximately 99.9%). Moreover, HC shows significantly improved high rate capability at rates of 3–20 C, compared to natural graphite (Fig. 2d). These outstanding cycling performance and superior rate capability of the HC may be mainly attributed to the nanoporous structure which provides much shorter diffusion pathways with lithium ions.⁴²

2.3. Synthesis and characterization of HC@c-Si@a-Si

As-prepared HC particles were coated by a-Si through CVD using silane (SiH₄) as the Si precursor (Schematic illustration in Fig. 3a). To verify this structure, SEM and focused ion beam (FIB) experiments were carried out. Amorphous Si uniformly covers the

surface of the HC and thickness of a-Si layer is about 50 nm (Fig. 3b and c). Furthermore, the elemental mapping image taken from Fig. 3d clearly shows elemental distribution of carbon core and Si shell in the HC@a-Si. From these results, we may conclude that the HC@a-Si was successfully synthesized by combining high-rate HC with high-capacity Si. However, when the a-Si layer in the outermost region is exposed to electrolytes during the battery operation, a serious side reaction may occur. Therefore, we introduced very thin carbon layers on the surface of the HC@a-Si by thermal decomposition of acetylene gas at 900 °C for 3 min.

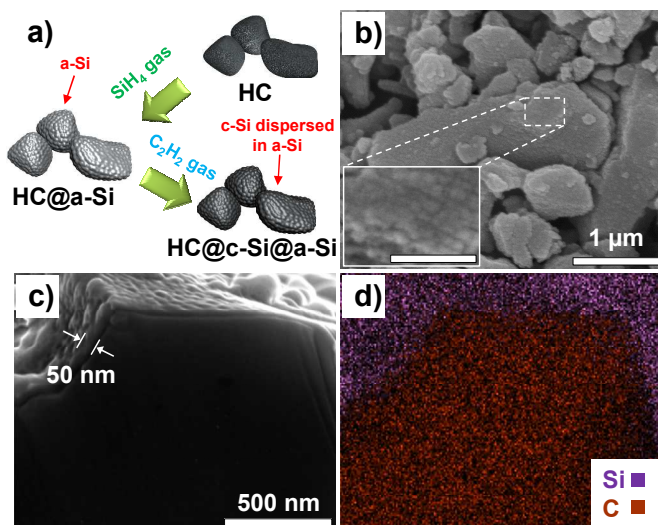


Fig. 3 Characterizations of as-prepared HC@c-Si@a-Si particles. (a) Schematic illustration of the HC@c-Si@a-Si, (b) SEM image of HC@c-Si@a-Si (inset: magnified SEM image showing Si coating layer in the HC@c-Si@a-Si particle. Scale bar in the inset is 100 nm.), (c) FIB-sectioned SEM image of the HC@c-Si@a-Si particle, (d) Energy dispersive X-ray mapping image of HC@c-Si@a-Si particle.

Advantages of carbon coating layer on the Si surface are well-known in other reports.^{43,44} Briefly, the carbon coating can improve the electrical conductivity of Si particles and make a stable SEI layer on the Si surface. Notably, a-Si can be partially transformed to c-Si above 600 °C.⁴⁵⁻⁴⁷ Thus, as a result of the carbon coating at 900 °C, we successfully synthesized carbon coated c-Si@a-Si encapsulated HC (HC@c-Si@a-Si) particles. To understand the morphology and microstructure of the HC@c-Si@a-Si, high resolution transmission electron microscopy (HR-TEM) was used. The thickness of the c-Si@a-Si layer is about 50 nm and uniformly covers the HC particles (Fig. 4a). The high-magnification TEM images further reveal that the nanodomains of crystalline silicon with an interlayer spacing of 0.310 nm (111) are uniformly dispersed in the a-Si regions and the thin carbon coating layer (about 3 nm) is also observed (Fig. 4b). The element analysis showed that HC@c-Si@a-Si consists of 20 wt % of Si and 80 wt% carbon.

XRD patterns and Raman spectra of the HC@c-Si@a-Si particles also support the presence of nanodomains of crystalline Si, as confirmed by HR-TEM. Fig. 4c shows the XRD patterns of the HC@a-Si particles before and after carbon coating process. The peaks due to Si diffractions are clearly observed in the XRD pattern of the carbon coated HC@c-Si@a-Si. On the contrary, very broad peaks corresponding to amorphous Si are detected in the HC@a-Si sample. Crystallite size of c-Si can be calculated using the Scherrer

equation.⁴⁸ The average size of the crystalline domains is calculated by Scherrer formula (1):

$$(1) \tau = K\lambda / \beta \cos \theta$$

Where K is a dimensionless shape factor, λ is the X-ray wavelength, β is the line broadening at half the maximum intensity, and θ is the Bragg angle. From the Scherrer formula, crystallite size of c-Si dispersed in a-Si layer is about 19.01 nm.

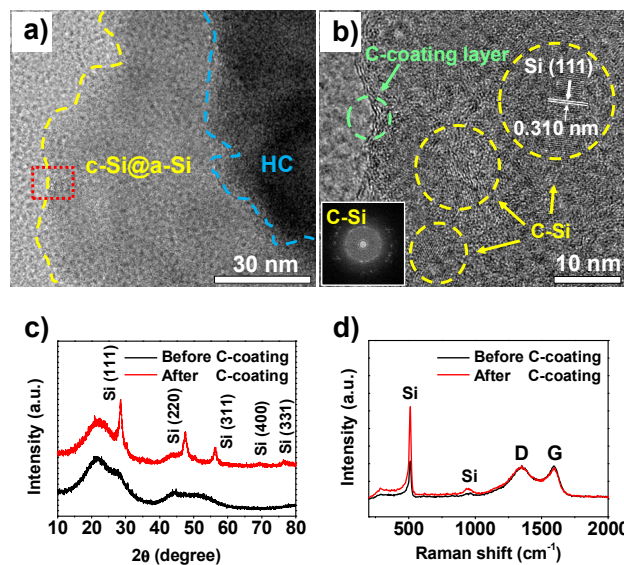


Fig. 4 HR-TEM images of (a) the HC@c-Si@a-Si after carbon coating; (b) the TEM image magnified from red box seen in (a) (inset: The Fast Fourier-Transform (FFT) image showing polycrystalline Si); (c) XRD patterns of the HC@a-Si before and after carbon coating, (d) Raman spectra of the HC@a-Si before and after carbon coating.

In Raman spectra, as the crystallization of the a-Si proceeds, peak intensity of Si is significantly increased, indicating that nanodomains of the c-Si were created in the a-Si phase (Fig. 4d).^{46,49}

2.4. Electrochemical performances of HC@c-Si@a-Si

The electrochemical properties of the HC@c-Si@a-Si were comparatively tested against HC/carbon coated nano-sized crystalline Si (~100 nm) composite (denoted as HC/n-Si).

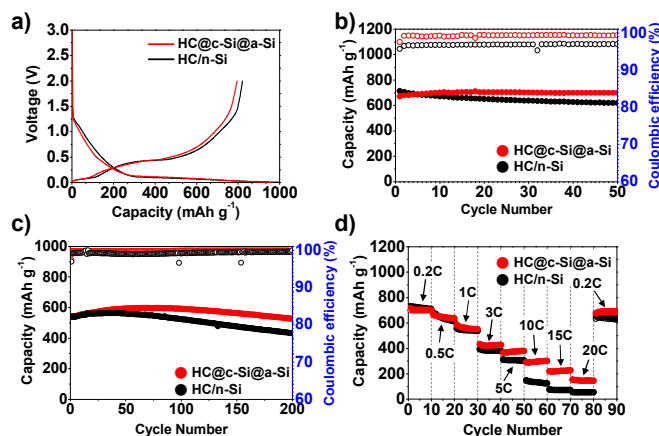


Fig. 5 Electrochemical performances of HC@c-Si@a-Si electrodes. (a) First discharge/charge curves of the HC@c-Si@a-Si and HC/n-Si at a rate of 0.05 C between 0.005 V and 2.0 V; Cycle performances of HC@c-Si@a-Si and HC/n-Si at a rate of (b) 0.2C and (c) 1C discharge/charge; (d) Rate capabilities of HC@c-Si@a-Si and HC/n-Si (the same discharge/charge rate was used from 1 to 20 C).

Carbon coating of n-Si was conducted via thermal decomposition method of acetylene gas at 900 °C for 3 min in the same way as the HC@c-Si@a-Si and thin carbon coating layer on n-Si (about 5 nm) is shown in TEM images (ESI, Fig. S1†).

Fig. 5a shows the first discharge/charge curves in the voltage window of 0.005–2 V (vs. Li/Li⁺) at a rate of 0.05 C (corresponding to 33 mA g⁻¹). The discharge capacity and charge capacity of the HC@c-Si@a-Si electrodes are 964.2 and 794.9 mAh g⁻¹ with 82.4 % of ICE. In case of the HC/n-Si electrodes, the discharge and charge capacity are 1025.53 and 821.2 mAh g⁻¹, respectively, with 80.0 % of ICE. Both electrodes show stable cycle retention at a low rate of 0.2 C discharge/charge. Whereas under the high rate of 1C discharge/charge, the HC@c-Si@a-Si electrodes showed much more improved cycle retention than the HC/n-Si electrodes (Fig. 5b and c). The capacity retention of the HC@c-Si@a-Si electrodes was 97.8% compared to the first cycle, while the HC/n-Si electrodes exhibited capacity retention of 81.6% after 200 cycles at a rate of 1 C discharge/charge.

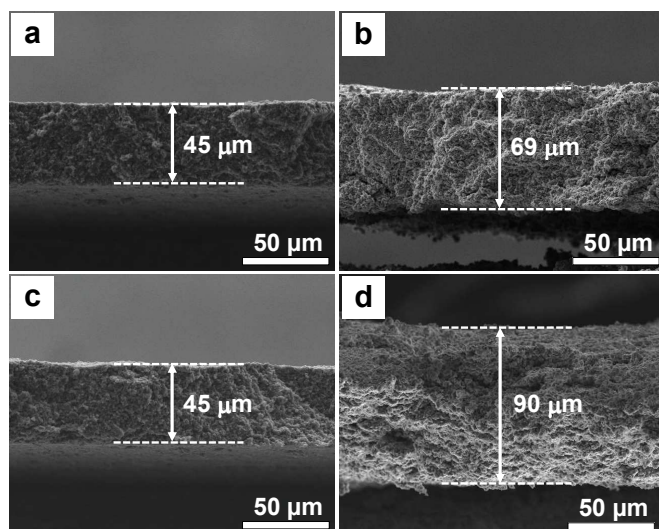


Fig. 6 Characterization of volume expansion. Cross-sectional SEM images of pristine electrodes ((a) HC@c-Si@a-Si electrode and (c) HC/n-Si) and electrodes after 200 cycles ((b) HC@c-Si@a-Si and (d) HC/n-Si).

Moreover, rate capabilities of both HC@c-Si@a-Si and HC/n-Si electrodes were examined at various discharge/charge rates (0.2C–20C), as shown in Fig. 5d. The HC@c-Si@a-Si electrodes show superior rate performance at various rates (the same discharge/charge rate) without notable capacity fading at each rate section and especially maintain far more improved capacity than the HC/n-Si electrodes under very high rates (10C–20C). Furthermore, when the rate is changed from 20 C back to 0.2 C, the specific capacities are almost fully recovered to its initial capacity at a rate of 0.2C. Such an outstanding cycle retention and rate capability of the HC@c-Si@a-Si electrodes may be explained by its components and structure. First, most parts of the Si shell in the HC@c-Si@a-Si was composed of the deformable a-Si. Cui's group reported that the

critical size for fracture of the a-Si is much larger than c-Si.³¹ They observed that the critical size of c-Si spheres for fracture was 150 nm in diameter and they also observed no fracture of a-Si spheres up to 870 nm in diameter. Their results indicate that a-Si is more deformable than c-Si. In our experiments, the thickness of the a-Si layer of the HC@c-Si@a-Si is only about 50 nm. Furthermore, the average size of the c-Si nanodomains is approximately 20 nm which is much smaller than critical fracture size of the c-Si spheres (150 nm in diameter) and they finely dispersed in the deformable a-Si layer. Thus, the Si layer of the HC@c-Si@a-Si is well maintained without a significant pulverization during the cycling. Second, the micron-sized HC@c-Si@a-Si particles have less chance to be isolated from conducting agent and binders than separated nano-Si particles in the HC/c-Si composites. In SEM image of the HC/n-Si electrodes, carbon coated n-Si particles are separated from the HC particles, while the shape of the HC@c-Si@a-Si particles is well preserved (ESI, Fig. S2†). It is well known that the capacity fading of Si anode is caused by pulverization of Si particles, and thereby creation of electrically isolated secondary particles.¹ As shown in Fig. 4a, amorphous Si is conformally coated on the surface of HC and maintains the structural integrity of the HC@c-Si@a-Si. This ideal structure prevents particles from pulverization during cycling even at the high current densities. From those results, the combination of the high rate HC particles and the high capacity c-Si@a-Si layers leads to the outstanding electrochemical performances including a high specific capacity, a long-term cycling stability, and good rate capabilities.

In addition to electrochemical properties of Si-based anode materials, volume expansion of the electrodes is one of the critical factors to use in practical LIB applications.^{50,51} Fig. 6 shows cross-sectional SEM images of both HC@c-Si@a-Si and HC/n-Si electrodes after 200 cycles at a rate of 1C discharge/charge. As expected, the HC@c-Si@a-Si electrodes show a significantly reduced volume expansion (53%), compared to that of the HC/n-Si electrodes (100%). It can be explained that the Si shell of the HC@c-Si@a-Si particles is effectively maintained without detachment from the HC core. On the contrary, n-Si particles (~200 nm in diameter) are only composed of crystalline Si and they are already separated from the HC in the HC/n-Si electrodes before cycling. Therefore, the n-Si particles undergo more severe pulverization and they are easily detached from the HC than a-Si. As a result, the volume expansion of the HC@c-Si@a-Si electrodes is much smaller than the HC/n-Si electrodes.

To further investigate the superior rate capabilities of the HC@c-Si@a-Si electrodes, electrochemical impedance spectroscopy (EIS) was conducted. The Nyquist impedance plots are obtained after 1st and after 200th cycle for each sample (ESI, Fig. S3†). The semicircle appearing in the high-frequency region is attributed to the existence of contact resistance by the formation of SEI layer.⁵² The medium-frequency semicircle is assigned to the charge transfer resistance, and the straight line in the low-frequency region corresponds to the mass transfer of lithium ions.^{53,54} The SEI film resistance (R_{SEI}) and charge-transfer resistance (R_{ct}) of the HC@c-Si@a-Si electrodes are smaller than those of HC/n-Si electrodes both after 1st and 200th cycle at a rate of 1C. The results indicate that the HC@c-Si@a-Si formed and maintained more stable SEI layer than HC/c-Si. Therefore, the structure of the HC@c-Si@a-Si is more suitable for the Li⁺ diffusion.

To confirm the effectiveness of the HC@c-Si@a-Si for practical use in LIB applications, the cycling and rate performance of the HC@c-Si@a-Si was conducted using coin-type (2016 R-type) full cells. LiCoO₂ was used as cathode materials in the full-cell test. The voltage profiles of the LiCoO₂/HC@c-Si@a-Si and LiCoO₂/HC/n-Si

cells at a rate of 1C charge/discharge in the range of 2.3–4.1 V are displayed in Fig. 7a and b.

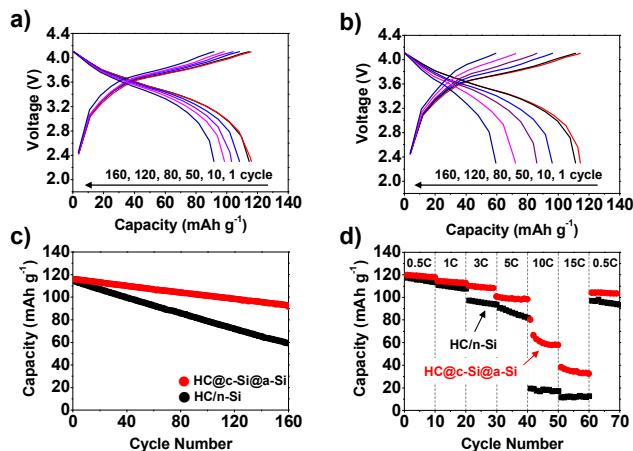


Fig. 7 Electrochemical performances of the LiCoO₂/HC@c-Si@a-Si and the LiCoO₂/HC/n-Si full-cells. Variation in the charge/discharge profiles of a) the LiCoO₂/HC@c-Si@a-Si and b) the LiCoO₂/HC/n-Si full cell during cycling; c) Cycle performances at a rate of 0.2 C discharge/charge and d) rate capabilities of both electrodes. The same discharge/charge rate was used from 0.2–20 C between 2.3–4.1 V.

The LiCoO₂/HC@c-Si@a-Si cell shows very slow degradation of its capacity during cycling. On the other hand, capacity of the LiCoO₂/HC/n-Si cell is rapidly reduced after few cycles. Fig. 7c is the long term cycling performance of the full cells at a rate of 1C discharge/charge in the range of 2.3–4.1 V. The capacity retention for the LiCoO₂/HC@c-Si@a-Si cell is 80% after 160 cycles. Meanwhile, the LiCoO₂/HC/n-Si cell shows more severe degradation of its capacity and only 52% of capacity retention is obtained after 160 cycles at the same rate. Similar aspects obviously appear in the rate performance test under at various rates ranging from 0.5 C to 15 C discharge/charge as well (Fig. 7d). The LiCoO₂/HC@c-Si@a-Si cell shows much improved capacity retention under high current density and almost fully recovers to its initial capacity at a rate of 0.2C after cycling at a rate of 15 C discharge/charge. These results are consistent with the results of above the half-cell test.

3. Conclusion

We have demonstrated that nanocrystalline Si dispersed in a-Si encapsulating hard carbon (HC@c-Si@a-Si) showed significantly improved cycle retention and superior rate capability as potential anode materials for LIBs. The hard carbon was derived from simple carbonization of natural polysaccharide (agarose) and subsequently coated by a-Si through CVD using silane (SiH₄) gas. In order to enhance electric conductivity and make stable SEI layer of the HC@a-Si, carbon coating was conducted via thermal decomposition method of acetylene, and meanwhile, c-Si nanodomains were naturally formed and uniformly dispersed in a-Si layer. This HC@c-Si@a-Si core-shell structures combine high capacity provided by c-Si@a-Si with the high electrical conductivity, long cycle life, and excellent rate performance of the hard carbon. In the electrochemical test, HC@c-Si@a-Si retained its capacity of 97.8% (versus the first cycle) after 200 cycles at a rate of 1 C discharge/charge and showed high capacity retention (54 % of its reversible capacity at 0.2 C rate) at a rate of 5 C discharge/charge. Furthermore, thin c-Si@a-Si layer uniformly covered the surface of HC was well maintained during the

cycling, resulting in a significant reduction of volume expansion (53%). In order to apply for real battery application, the full-cell test was conducted. The LiCoO₂/HC@c-Si@a-Si full-cell delivered more than half of its capacity at a rate of 10 C discharge/charge and showed more stable cycle retention of 80 % after 160 cycles at a rate of 1 C discharge/charge. This effective strategy may be extended to other anodes materials for next generation LIBs.

Acknowledgements

This work was supported by the MSIP (NIPA-2013-H0301-13-1009) program and the BK21 Plus funded by the Ministry of Education, Korea (META-material-based Energy Harvest and Storage Technologies, 10Z20130011057).

Notes and references

^a School of Energy and Chemical Engineering, Ulsan National Institute of Science and Technology (UNIST), 50 UNIST-gil, Ulju-gun, Ulsan 689-798, Republic of Korea

E-mail: jpcho@unist.ac.kr, spark@unist.ac.kr

^b Department of Chemical Engineering, Kangwon National University, Chuncheon, Kangwondo, 200–701, South Korea

† Electronic Supplementary Information (ESI) available: HRTEM image of coated nano-sized crystalline Si, SEM image of pristine electrodes, Nyquist plots of the electrochemical impedance spectra of electrodes. See DOI:10.1039/xxxx

- M. T. McDowell, S. W. Lee, W. D. Nix, Y. Cui, *Adv. Mater.*, 2013, **25**, 4966–4985.
- Y. Xu, Q. Liu, Y. Zhu, Y. Liu, A. Langrock, M. R. Zachariah, C. Wang, *Nano Lett.*, 2013, **13**, 470–474.
- M. Wu, J. E. Sabisch, X. Song, A. M. Minor, V. S. Battaglia, G. Liu, *Nano Lett.*, 2013, **13**, 5397–5402.
- F. M. Hassan, V. Chabot, A. R. Elsayed, X. Xiao, Z. Chen, *Nano Lett.*, 2014, **14**, 277–283.
- H. Wu, G. Yu, L. Pan, N. Liu, M. T. McDowell, Z. Bao, Y. Cui, *Nature Commun.*, 2013, **4**, 1943.
- S. Sim, P. Oh, S. Park, J. Cho, *Adv. Mater.*, 2013, **25**, 4498–4503.
- J. Deng, H. Ji, C. Yan, J. Zhang, W. Si, S. Baunack, S. Oswald, Y. Mei, O. G. Schmidt, *Angew. Chem. Int. Ed.*, 2013, **52**, 2326–2330.
- F. Wang, L. Wu, B. Key, X.-Q. Yang, C. P. Grey, Y. Zhu, J. Graetz, *Adv. Energy Mater.*, 2013, **3**, 1324–1331.
- M. E. Stourmar, X. Xiao, Y. Qi, P. Johari, P. Lu, B. W. Sheldon, H. Gao, V. B. Shenoy, *Nano Lett.*, 2013, **13**, 4759–4768.
- J. T. Lee, N. Nitta, J. Benson, A. Magasinski, T. F. Fuller, G. Yushin, *Carbon*, 2013, **52**, 388–397.
- C. K. Chan, H. L. Peng, G. Liu, K. McIlwrath, X. F. Zhang, R. A. Huggins, Y. Cui, *Nat. Nanotechnol.*, 2008, **3**, 31–35.
- R. Huang, X. Fan, W. C. Shen, J. Zhu, *Appl. Phys. Lett.*, 2009, **95**, 133119.
- H. Kim, M. Seo, M. H. Park, J. Cho, *Angew. Chem. Int. Ed.*, 2010, **49**, 2146–2149.
- R. Teki, M. K. Datta, R. Krishnan, T. C. Parker, T. M. Lu, P. N. Kumta, N. Koratkar, *Small*, 2009, **5**, 2236–2242.
- A. Magasinski, P. Dixon, B. Hertzberg, A. Kvit, J. Ayala, G. Yushin, *Nat. Mater.*, 2010, **9**, 461.

- 16 S. Choi, J. C. Lee, O. Park, M. J. Chun, N. S. Choi, S. Park, *J. Mater. Chem. A*, 2013, **1**, 10617-10621.
- 17 C.-H. Yim, F. M. Courtel, Y. Abu-Lebdeh, *J. Mater. Chem. A*, 2013, **1**, 8234-8243.
- 18 D. Shao, D. Tang, Y. Mai, L. Zhang, *J. Mater. Chem. A*, 2013, **1**, 15068-15075.
- 19 W. Wang, P. N. Kumta, *Acs Nano*, 2010, **4**, 2233-2241.
- 20 J. Song, S. Chen, M. Zhou, T. Xu, D. Lv, M. L. Gordin, T. Long, M. Melnyk, D. Wang, *J. Mater. Chem. A*, 2014, **2**, 1257-1262.
- 21 Q. Xiao, Y. Fan, X. Wang, R. A. Susantyoko, Q. Zhang, *Energy Environ. Sci.*, 2014, **7**, 655-661.
- 22 H. Uono, B.-C. Kim, T. Fuse, M. Ue, J.-i. Yamaki, *J. Electrochem. Soc.*, 2006, **153**, A1708- A1713.
- 23 T. Zhang, J. Gao, L. J. Fu, L. C. Yang, Y. P. Wu, H. Q. Wu, *J. Mater. Chem.*, 2007, **17**, 1321- 1325.
- 24 T. Zhang, J. Gao, H. P. Zhang, L. C. Yang, Y. P. Wu, H. Q. Wu, *Electrochem. Commun.*, 2007, **9**, 886-890.
- 25 D. Wang, M. Gao, H. Pan, J. Wang, Y. Liu, *J. Power Sources*, 2014, **256**, 190-199.
- 26 Y. He, X. Yu, Y. Wang, H. Li, X. Huang, *Adv. Mater.*, 2011, **23**, 4938-4941.
- 27 Z. Zhang, M. Zhang, Y. Wang, Q. Tan, X. Lv, Z. Zhong, H. Li, F. Su, *Nanoscale*, 2013, **5**, 5384-5389.
- 28 J. Wang, Y. Tong, Z. Xu, W. Li, P. Yan, Y.-W. Chung, *Mater. Lett.*, 2013, **97**, 37-39.
- 29 G. A. Tritsarlis, K. Zhao, O. U. Okeke, E. Kaxiras, *J. Phys. Chem. C*, 2012, **116**, 22212-22216.
- 30 C. C. Nguyen, S.-W. Song, *Electrochim. Acta*, 2010, **55**, 3026-3033.
- 31 M. T. McDowell, S. W. Lee, J. T. Harris, B. A. Korgel, C. Wang, W. D. Nix, Y. Cui, *Nano Lett.*, 2013, **13**, 758-764.
- 32 A. Piotrowska, K. Kierzek, P. Rutkowski, J. Machnikowski, *J. Anal. Appl. Pyrolysis*, 2013, **102**, 1-6.
- 33 J. Tang, J. Yang, X. Zhou, *Mater. Lett.*, 2013, **109**, 253-256.
- 34 Z. H. Yi, Y. G. Liang, X. F. Lei, C. W. Wang, J. T. Sun, *Mater. Lett.*, 2007, **61**, 4199-4203.
- 35 J. Biener, S. Dasgupta, L. H. Shao, D. Wang, M. A. Worsley, A. Wittstock, J. R. I. Lee, M. M. Biener, C. A. Orme, S. O. Kucheyev, B. C. Wood, T. M. Willey, A. V. Hamza, J. Weissmuller, H. Hahn, T. F. Baumann, *Adv. Mater.*, 2012, **24**, 5083-5087.
- 36 C. Kim, S. H. Park, J. K. Cho, D. Y. Lee, T. J. Park, W. J. Lee, K. S. Yang, *J. Raman Spectrosc.*, 2004, **35**, 928-933.
- 37 B. Wang, X. Li, T. Qiu, B. Luo, J. Ning, J. Li, X. Zhang, M. Liang, L. Zhi, *Nano Lett.*, 2013, **13**, 5578-5584.
- 38 Y. H. Liu, J. S. Xue, T. Zheng, J. R. Dahn, *Carbon*, 1996, **34**, 193-200.
- 39 L. C. Zhang, Z. Hu, L. Wang, F. Teng, Y. Yu, C. H. Chen, *Electrochim. Acta*, 2013, **89**, 310-316.
- 40 J. R. Dahn, T. Zheng, Y. H. Liu, J. S. Xue, *Science*, 1995, **270**, 590.
- 41 E. Buiel, J. R. Dahn, *Electrochim. Acta*, 1999, **45**, 121-130.
- 42 J. Yang, X. Y. Zhou, Y. L. Zou, J. J. Tang, *Electrochim. Acta*, 2011, **56**, 8576-8581.
- 43 S. H. Ng, J. Z. Wang, D. Wexler, K. Konstantinov, Z. P. Guo, H. K. Liu, *Angew. Chem. Int. Ed.*, 2006, **45**, 6896-6899.
- 44 R. Yi, F. Dai, M. L. Gordin, H. Sohn, D. H. Wang, *Adv. Energy Mater.*, 2013, **3**, 1507-1515.
- 45 K. Sharma, A. Branca, A. Illiberi, F. D. Tichelaar, M. Creatore, M. C. M. van de Sanden, *Adv. Energy Mater.*, 2011, **1**, 401-406.
- 46 O. T. Ozmen, M. Karaman, R. Turan, *Thin Solid Films*, 2014, **551**, 181-187.
- 47 S. I. Jun, P. D. Rack, T. E. McKnight, A. V. Melechko, M. L. Simpson, *Appl. Phys. Lett.*, 2006, **89**, 022104.
- 48 B. D. Cullity, *Elements of X-Ray Diffraction*, Addison-Wesley, MA, 1978.
- 49 Y. J. Lee, J. D. Kwon, D. H. Kim, K. S. Nam, Y. Jeong, S. H. Kwon, S. G. Park, *Thin Solid Films*, 2013, **542**, 388-392.
- 50 H. J. Lin, W. Weng, J. Ren, L. B. Qiu, Z. T. Zhang, P. N. Chen, X. L. Chen, J. Deng, Y. G. Wang, H. S. Peng, *Adv. Mater.*, 2014, **26**, 1217-1222.
- 51 X. Su, Q. L. Wu, J. C. Li, X. C. Xiao, A. Lott, W. Q. Lu, B. W. Sheldon, J. Wu, *Adv. Energy Mater.*, 2014, **4**, 23.
- 52 C. Kim, J. Y. Jang, N. S. Choi, S. Park, *RSC Adv.*, 2014, **4**, 3070-3074.
- 53 S. Xu, C. M. Hessel, H. Ren, R. Yu, Q. Jin, M. Yang, H. Zhao, D. Wang, *Energy Environ. Sci.*, 2014, **7**, 632.
- 54 S. H. Choi, Y. C. Kang, *ChemSusChem*, 2013, **6**, 2111-2116.